Journal of CO2 Utilization 81 (2024) 102705

Contents lists available at ScienceDirect

Journal of CO2 Utilization

journal homepage: www.elsevier.com/locate/jcou

Modeling and optimization of atmospheric CO_2 capture for neutralization of high alkaline wastewaters using response surface methodology

Luís Madeira [a,b,c], Margarida Ribau Teixeira [a,c,*], Fátima Carvalho [b,c,d]

[a] Faculdade de Ciências e Tecnologia, Universidade do Algarve, Edifício 7, Campus de Gambelas, Faro 8005-139, Portugal
[b] Departamento de Tecnologias e Ciências Aplicadas, IPBeja, Ap. 158, Beja 7801-902, Portugal
[c] CENSE, Center for Environmental and Sustainability Research, Portugal & CHANGE, Global Change and Sustainability Institute, Portugal
[d] FiberEnTech, Fiber Materials and Environmental Technologies, Universidade de Beira Interior, Covilhã, Portugal

ARTICLE INFO

Keywords:
Atmospheric CO_2 capture
Alkaline wastewater
Capillary action
Stirrer bubble column
Slaughterhouse

ABSTRACT

Lab-scale stirrer bubble and lab-scale stepped continuous flow capillary columns were developed to neutralize lime precipitation treated slaughterhouse wastewater (SWW) and recover the volatilized ammonia, using atmospheric CO_2. These experiments were carried out using central composite design based on the response surface methodology. The carbonation process occurred in both processes. For the bubbling process, numerical optimization indicated a final pH of 8 with calcium and ammonium nitrogen removals of 76.0 and 66.2%, respectively, applying 21 h, air flow rate at 65 L h^{-1}, the stirring speed at 52 rpm, and SWW volume at 178 mL. It was also observed that increasing the air flow rate can avoid the stirring step. For the capillary process, a pH of 8.2 and calcium and ammonium nitrogen removals of 81.0 and 57.5% were achieved, applying a SWW flow rate at 1.2 mL min^{-1}, air flow rate at 90 L h^{-1}, and capillary area at 700 cm^2. Under optimal conditions, the flow capillary column was able to neutralize different SWW volumes, 178–478 mL, without significant differences in the collected samples, with the operation time varying between 4.48 and 10.20 h, respectively.

1. Introduction

Carbon neutrality is on the global agenda. Carbon capture and storage (CCS) and direct air capture (DAC) are technologies that can contribute to this neutrality [1–4]. CCS has been widely explored. Different solvents such as alkaline solutions (e.g., CaO [5], piperazine solution [6], Sr and Ba alkaline solutions [7], NaOH [8,9], and others), alcohols (e.g., methanol, ethanol, 2-Propanol, and others) [10], amine-based solvents (e.g., diethanolamine solutions) [11–13] and alkaline wastewaters [14,15] have been tested to capture CO_2 from industrial flue gases or simulated flue gases. However, the neutralization of high alkaline wastewater [16–25] by DAC still needs further investigation. DAC is more interesting than the use of strong acids because CO_2 is not corrosive, allows greater control in the pH drop, there is anywhere, and contribute for reducing the carbon footprint of wastewater treatment plants [26–28]. Moreover, unlike alkaline solutions, it is expected that DAC is less expensive since no decarbonization step is necessary as wastewaters are sent for disposal or reuse [29,30]. DAC for neutralization of high alkaline wastewaters has been a challenge because unlike the CCS, it takes a long time, given the low concentration of CO_2 in the atmosphere compared to CO_2-containing flue gases [14,31]. Different gas−liquid contactors have been investigated [9,32–36]. Long carbonation time ($\geq$ 7 days) to reduce the effluent pH from 12 to 8 by DAC has been observed using static and open reactor [29,37–39]. In these systems, the effluent remains stable over time while its surface is in contact with atmospheric air [40]. Low area/volume ratio of reactor used ($\leq$ 7 m^2/m^3), and the presence of the lime precipitation process precipitate during the carbonation process [29] may justify the high carbonation time in these systems. Aeration tank has contributed to better mixing of atmospheric air and liquid by injecting air in the form of bubbles, resulting a lower time carbonation [41,42]. Correia et al. [42] reduced the carbonation time from 220 to 100 hours in the neutralization of an alkaline urban effluent pretreated at pH 11.5 by DAC using an aeration tank (with air flow at 85 L h^{-1}). However, as the carbonation process is performed in an open system, if the ammonia is present in the effluent it may be released into the atmosphere [29,39]. Thus, there is a necessity to develop new cost-effective ways to promote a greater liquid-air interface for DAC in closed systems. Stirred bubble column (SBC) is a technology recognized for its high CO_2 absorption capacity derived from the large gas-liquid contact area caused by the stirring

* Corresponding author at: Faculdade de Ciências e Tecnologia, Universidade do Algarve, Edifício 7, Campus de Gambelas, Faro 8005-139, Portugal.
E-mail address: mribau@ualg.pt (M. Ribau Teixeira).

https://doi.org/10.1016/j.jcou.2024.102705
Received 10 November 2023; Received in revised form 17 January 2024; Accepted 12 February 2024
Available online 20 February 2024

speed [6]. Pashaei et al. [11] observed that increasing the stirring speed favors higher CO_2 absorption rates into aqueous solution of diethanolamine. On the other hand, under constant stirring speed, Liendo et al. [5] observed a rapid drop in pH when the authors increased the flue gas flow to neutralize CaO slurry. To the best of our knowledge, it is unknown whether increasing air flow (which also contributes to effluent turbulence) could reduce or even avoid the stirring step to reduce the energy costs associated, which unlike CCS, can be significant for DAC due to its long carbonation time. On the other hand, it is unknown whether the stirring and bubbling steps could be sucessfully replaced by gravitational displacement or by siphon-driven of alkaline wastewater onto a surface with capillary characteristics that promote larger gas-liquid contact area. This process has contributed to the metal (e.g., iron [43,44] and manganese [45]) and organic contaminants removals [46], and water desalination [47]. However, to the best of our knowledge, the use of this process for alkaline wastewater neutralization purposes as well as its effectiveness with increasing the volume of effluent processed, has not been reported. To fill these gaps, this work aims to develop and model the DAC for neutralizing high alkaline wastewater resulting from lime precipitation, and recovering volatilized ammonia, using two new closed systems. A system based on bubbling and agitation of the effluent (hereinafter referred to as SBC) and another system based on the continuous displacement of the effluent over a capillary (hereinafter referred to as stepped continuous flow capillary column (SCFCR)) were used. Response surface methodology (RSM) was used to evaluate the interactive effects between two or more experimental variables on the response variables. RSM has been applied to model various wastewater treatment processes, as it allows: i) finding the best model that can predict the response variables through mathematical equations, ii) identifying the independent variables that affect the response variables, iii) finding the best operating conditions through the optimization process, and iv) validate the RSM model based on statistical criteria [48].

2. Materials and methods

2.1. Raw and pretreated slaughterhouse wastewater (SWW)

Raw slaughterhouse wastewater (SWW) was collected from the output of the rotary drum screen filter in a slaughterhouse located in Portugal. Then, raw SWW was treated by immediate one-step lime precipitation (IOSLM) at pH 12 using calcium hydroxide ($\geq$ 95%, PanReac S.A), according to Madeira et al. [20]. The pretreated SWW samples were characterized in terms of pH, conductivity, calcium, total alkalinity, and ammonium nitrogen. If not immediately analyzed, the collected samples were stored at 4 ºC until use. The SWW characteristics are provided in Table 1. According to Table 1, the effluents used are characterized by high pH (around 12), conductivity (around 5 mS cm^{-1}), and calcium (between 500 and 600 mg L^{-1}), which are characteristics of the effluents after the IOSLM process, and contains substantial amounts of ammonium nitrogen (between 60 and 80 mg N-NH_4^+ L^{-1}).

Table 1
Physicochemical characterization of pretreated SWW resulting from IOSLM at pH 12.

Parameter	Unit	Used in experiments of:	
		Bubbling process	Capillary process
pH	Sorensen scale	11.88±0.05	12.13±0.02
Conductivity	mS cm^{-1}	5.23±0.15	5.03±0.34
Calcium	mg L^{-1}	633.1±18.6	509.7±7.6
Total alkalinity	mg $CaCO_3$ L^{-1}	1614±0	1296±0
Ammonium nitrogen	mg N-NH_4^+ L^{-1}	84.5±0.9	61.7±1.4

2.2. Experimental setup and procedure

Before carrying out the experiments, the stability of the reactors was guaranteed by analyzing the coefficient of determination at 95% level of confidence on a set of pH measurements obtained under different operating conditions. Then, the experimental tests of atmospheric CO_2 carbonation were conducted in three experiments.

In the first experiment, the bubbling process took place (Fig. 1a). Between 178 and 478 mL of pretreated SWW was added to a lab-scale SBC (bottle column volume 750 mL and diameter 6.8 cm), under variable magnetic stirring (NORMAX® NX1200) (0–200 rpm) and atmospheric air injection (60–120 L h^{-1}) by an air pump (Marina® 75, Marina® 100, and Marina® 200). The reactor was hermetically sealed. The injected air was dispersed continuously (during 2–21 h) in the effluent by a bubble air diffuser (length 2.7 cm and diameter 1.3 cm) which was immersed in the bottle column. Then, the air was collected at the bottom of a beaker (height 35.3 cm and diameter 6 cm) containing 1 L of a sulfuric acid solution at pH 5, under dispersion by a bubble air diffuser (length 2.7 cm and diameter 1.3 cm). After the established time, the effluent was sedimented for 30 minutes and then analyzed according to Section 2.4.

In the second experiment, the capillary process was used (Fig. 1b). The pretreated SWW was gravitationally displaced, through a capillary located inside the lab-scale SCFCR (length, width, and height of 18.5, 14.5, and 35 cm, respectively), Fig. 1b, while atmospheric air was continuously injected using an air pump (Marina® 100, and Marina® 200) at 90–270 L h^{-1}. The pretreated SWW flow rate used varied between 1.2 and 2.0 mL min^{-1} and was controlled by a flow regulation valve and by the height of the water level in the pretreated SWW feed tank. The SCFCR was hermetically sealed. The capillary material used was a commercial non-woven compress (Pingo doce®) (width 5 cm, area 150–700 cm^2, and thickness 1 mm), non-sterile, with high absorption capacity, composed of four layers made of 70% viscose and 30% polyester, which was arranged in a zigzag pattern with a slope of 17.7% in the SCFCR. The SCFCR injected air was collected in a beaker (height 35.3 cm and diameter 6 cm) filled with 1 L of sulfuric acid solution (at pH 5) and with a bubble air diffuser (length 2.7 cm and diameter 1.3 cm). After collecting 50 mL of effluent from the SCFCR, the experiment was terminated and the sample was analyzed according to Section 2.4.

Finally, in the third experiment, the capillary process was performed again to evaluate the efficiency of the process in obtaining different volumes collected. Thus, 178, 328, and 478 mL of pretreated SWW were collected, using the best conditions found in the previous tests.

For both processes, the ammonia capture capacity was analyzed using the optimized conditions defined according to the selected criteria for independent variables and response variables (see Section 2.3). The samples were analyzed according to Section 2.4.

Throughout these experimental tests, the indoor air quality status (Table 2) was monitored (see Section 2.4).

2.3. Experimental design, optimization, and statistical analysis

In this work, the bubbling and the capillary experiments were carried out based on the RSM using the full face central composite design (CCD). RSM was used to analyze the effect of independent variables and their interactions on response variables, design experiments, build models, and find optimal operating conditions, through Design Expert 11 software (version 11.1.2.0).

A set of independent variables with a possible potential effect on the transfer of atmospheric CO_2 to the aqueous phase was proposed and evaluated for both processes. Four independent variables, aeration time, air flow rate, stirring speed, and SWW volume were performed for the bubbling process, while three variables, SWW flow rate, capillary area, and air flow rate, were for the capillary process. This set of variables was chosen for the following reasons. Aeration time has been the main

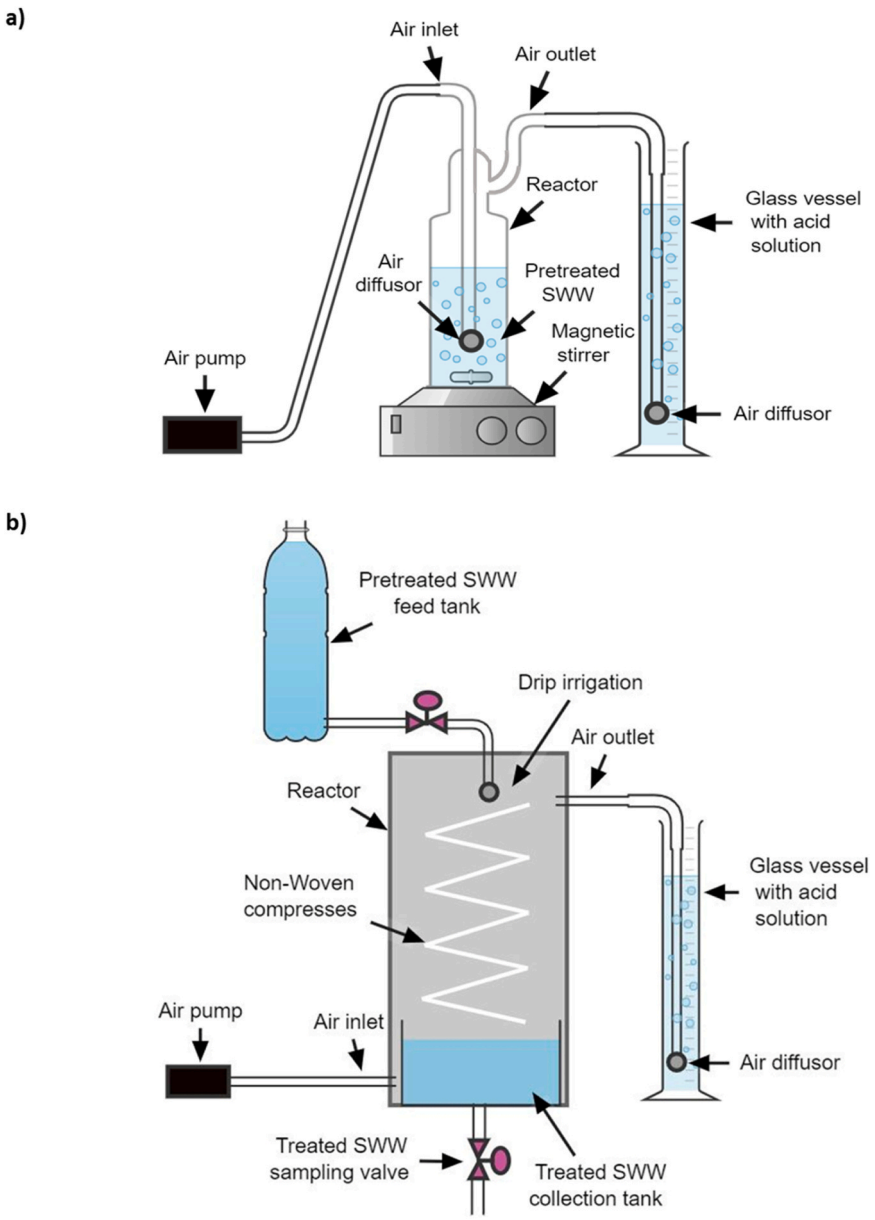

Fig. 1. Schematic diagrams of experimental systems relating to the atmospheric CO_2 carbonation process: a) stirrer bubble column and b) stepped continuous flow capillary column.

Table 2
Indoor air quality states during the experiments.

Parameter		Experiments	
		Bubbling process	Capillary process
Temperature (ºC)	Min.	14.3	19.6
	Mean	15.9	19.8
	Max.	16.5	20.3
CO_2 (mg L^{-1})	Min.	222	206
	Mean	288	271
	Max.	389	420

variable studied in atmospheric carbonation processes. Shorter times may be associated with lower CO_2 capture and energy costs (e.g. running an air pump), and vice versa. Agitation may be a variable that promotes a greater area of gas-liquid contact since standing liquids result in less gas exchange with water. The air flow can be an important variable in the renewal of the air in closed systems, in addition to allowing a greater area of contact between the gas and the liquid as has been observed in the aeration tanks. On the other hand, larger volumes of effluent to be treated may be associated with a smaller space of contact between the air and the liquid inside the closed system, as well as greater needs for the capture of atmospheric CO_2. The capillary area is the contact medium between the gas and the liquid. Finally, the pretreated SWW flow rate is a variable that is related to the aeration time and the volume to be treated, as already mentioned before. Each of these variables was coded at three levels (−1, 0, +1), whose studied range is shown in Table 3. pH, conductivity, calcium, total alkalinity, and ammonium nitrogen were the response variables.

The experimental conditions are shown in Tables S1 and S2 for the bubbling and the capillary processes, respectively. These experimental matrices of capillary and bubbling processes are composed of 19 (with 5 central points and 14 non-central points) and 30 experiments (with 6 central points and 24 non-central points), respectively. The central point was repeated 5 (for the capillary process) and 6 times (for the bubbling process) to determine the experimental deviation between them,

Table 3
Experimental range and levels of the independent variables in the bubbling and capillary processes.

Process	Independent variable	Symbol	Coded levels		
			-1	0	1
Bubbling	Time (h)	A	2	11.5	21
	Air flow rate (L h^{-1})	B	60	90	120
	Stirring speed (rpm)	C	0	100	200
	SWW volume (mL)	D	178	328	478
Capillary	SWW flow rate (mL min^{-1})	A	1.2	1.6	2.0
	Air flow rate (L h^{-1})	B	90	180	270
	Capillary area (cm^2)	C	150	425	700

providing more robust statistical support to the results.

A quadratic model was applied for both processes to model the relationship between response variables and the independent variables, using the following second-order polynomial Eq. (1):

$$Y = \beta_0 + \sum_{i=1}^{n} \beta_i x_i + \sum_{i=1}^{n} \beta_{ii} x_i^2 + \sum_{i=1}^{n-1} \sum_{j=i+1}^{n} \beta_{ij} x_i x_j \quad (1)$$

where Y is the response variable, x_i and x_j are coded independent variables, and β_0, β_i, β_{ii}, and β_{ij} are coefficients of intercept, linear, quadratic, and interaction terms, respectively. The model was evaluated by R^2 and F values. Subsequently, the model was validated for its reproducibility of results by repeating (in triplicate) an experiment carried out under optimal conditions. Once the model was validated, three-dimensional response surface graphs and contour plots were obtained.

The optimization was performed according to the constraint conditions defined for the response variables and independent variables, for both processes. All response variables were limited by the range of current values defined by Tables S1 and S2, respectively, except for pH. For pH, the target pH value was based on the minimum pH value found, and the upper limit of the range was restricted to 8.5 since it is the maximum pH value usually used in biological treatment. Regarding the independent variables, all of these were limited by their levels (established in Table 3), except when some variable was designated to minimize energy costs because it is a variable that does not have a significant effect on most parameters responses analyzed.

To confirm the statistical significance of the model, the effects of the input variables, and the interactions between the variables in the response, an analysis of variance (ANOVA) was performed with a *P*-value at the confidence level of 95%, using the Design Expert software. GraphPad Prism for Windows (version 8.0.1) was used to draw the graphs. XLSTAT 2022 statistical software (version 2022.2.1) was used to correlate the response variables.

2.4. Analytical methods

All chemical analyses were performed following the Standard Methods [49]. pH was measured by the potentiometric method, using WTW InoLab pH Level 1 apparatus and a pH electrode SenTix® 41. Electrical conductivity was determined by the electrometric method, using a Jenway 4510 conductivity meter and a conductivity sensor VWR phenomenal CO 11. Ammonium nitrogen was measured by distillation method using a nitrogen distillation unit BUCHI B-316, followed by titration with hydrochloric acid. Calcium was measured by volumetric complexation with EDTA, using a calcon indicator. Total alkalinity was determined by neutralization titration.

Indoor air quality was assessed by a 3 M™ EVM 7 Environmental Monitor Kit, which is a portable device whose measurement is continuous and in real-time. This equipment is equipped with a junction diode sensor and a non-dispersive infrared sensor for measuring temperature and carbon dioxide concentration levels, respectively, over a defined time interval.

In this work, the devices used were associated with the following accuracy values: ±100 ppm (20ºC, 1 bar pressure at 2000 ppm applied gas) for CO_2 sensor; ±1.1ºC for temperature sensor; ±0.01 for WTW InoLab pH Level 1 apparatus; 0.5% for Jenway 4510 conductivity meter; and ±8% for SWW flow rate.

3. Results and discussion

3.1. Statistical analysis of the overall model

The actual and predicted values of the different response variables referring to the experimental conditions applied to the bubbling process (Table S1 and Fig. S1) and the capillary process (Table S2 and Fig. S2) were obtained. Overall, the actual and predicted values were quite close. These similarities are confirmed by the proximity of most of the points to the diagonal axis (Figs. S1 and S2), indicating that the quadratic polynomial models chosen seem suitable to predict the response variables of both processes. The quadratic model adequacy was evaluated for different response variables using ANOVA (Table S3), both for the bubbling process and for the capillary process. According to Table S3, the models defined for pH, conductivity, calcium, and ammonia have excellent reproducibility (CV $\leq$ 10%), while the model defined for total alkalinity has good reproducibility (CV between 10% and 20%), for both processes. High determination coefficient (R^2) values were obtained ($\geq$ 0.96 for the bubbling process and $\geq$ 0.97 for the capillary process), indicating a high correlation between the predicted and actual values, for all response variables. Furthermore, high predicted R^2 values ($\geq$ 0.86 for the bubbling process and $\geq$ 0.89 for the capillary process) were obtained, indicating that the regression model can make predictions. For all response variables and both processes, the *P*-value was less than 0.05 ($P < 0.0001$), which suggest that the quadratic model was significant for all response variables.

3.2. Experimental design

As a result of the experimental conditions, the pH, conductivity, calcium concentration, total alkalinity, and ammonium nitrogen concentration ranged from 7.90 to 11.95, 1.5–5.3 mS cm^{-1}, 129–634 mg L^{-1}, 23–1401 mg $CaCO_3$ L^{-1}, and 24–86 mg N L^{-1}, respectively, in the bubbling process (Table S1). Regarding the capillary process (Table S2), the values varied between 8.16 and 12.04 for pH, 1.26 and 3.78 mS cm^{-1} for conductivity, 86 and 311 mg L^{-1} for calcium, 177 and 742 mg $CaCO_3$ L^{-1} for total alkalinity, and 22 and 45 mg N L^{-1} for ammonium nitrogen concentration. Minimum pH values observed around neutrality (of 7.90 and 8.16 for the bubbling process and the capillary process, respectively) indicated that there were experimental conditions that led to the occurrence of the carbonation process. On the other hand, the maximum pH values obtained (which practically correspond to the initial values of the effluent, Table 1), clearly indicate that carbonation process did not occur in both processes. The non-occurrence of the carbonation process happens when the calcium concentration is limited [39], which was not the case since high pH values were associated with high calcium concentrations. According to Viswanaathan et al. [31], temperature and atmospheric CO_2 concentration are factors that can influence the carbonation process. However, in this work the concentration of CO_2 was not limiting and no variation in temperature was observed so the dissolution of atmospheric CO_2 in the solution was prevented (Table 2). As the atmospheric carbonation process occurs in a closed system, the most plausible reason is the inability of certain operating conditions to disable the atmospheric carbonation process from occurring, as will be seen later in Section 3.3.

3.3. Effects of model parameters on response variables

For the bubbling and capillary processes, the individual and interactive effects of independent variables on pH, conductivity, calcium, total alkalinity, and ammonium nitrogen were evaluated by the second-

order polynomial equations (Table 4, Y_1 to Y_5 for the bubbling process and Y_6 to Y_{10} for the capillary process) and their coefficients (Tables S4 and S5), as well as their significance level (Tables S6 and S7).

3.3.1. Individual effects

Model components such as *A* (i.e., time), *B* (i.e., air flow rate) *C* (i.e., stirring speed), and *D* (i.e., SWW volume) for the bubbling process, and *A* (i.e., SWW flow rate), *B* (i.e., air flow rate), and *C* (i.e., capillary area) for the capillary process, represent the linear effects of the main independent variables. From Table S4, the model components such as *A*, *B,* and *C* in the bubbling process appear to contribute to the reduction of pH, conductivity, calcium, total alkalinity, and ammonia. ANOVA results (Table S6) indicate that all these contributions are significant ($P<0.05$), except for model component *B* on pH, conductivity, and calcium. In fact, the perturbation plot (Fig. 2) shows that the increase in time (curve A, from 2 to 21 h) and in stirring speed (curve *C*, from 0 to 200 rpm) contributes to the decrease in pH (Fig. 2a1), conductivity (Fig. 2b1), calcium (Fig. 2c1), total alkalinity (Fig. 2d1), and ammonium nitrogen (Fig. 2e1). Moreover, it is possible to observe that the time variable (curve *A*) was the independent variable that had the greatest influence on response variables, given its more accentuated curvature (Fig. 2a1–e1). Time has been a determining factor in the carbonation process in open systems [29,37–39,42,50]. On the other hand, the stirring speed favors higher CO_2 absorption rates into aqueous solution [11]. Although the turbulence at the water surface observed in the bubbling process can be created by the air flow rate and the stirring speed variables, contributing to the gas-liquid contact, the stirring speed had a greater effect on the response variables than the air flow rate (Fig. 2a1–e1).

The air flow rate applied (curve *B*, from 60 to 120 L h^{-1}) affect only the total alkalinity and ammonium nitrogen which decreased slightly at 60–90 L h^{-1} (Fig. 2d1) and at 90–120 L h^{-1} (Fig. 2e1), respectively. The variable air injection has deserved importance in the carbonation process in open systems as it contributes to a significant reduction in the carbonatation time of effluent treated by IOSLM [42]. Correia et al. [42] observed that the carbonation time of urban effluent treated by lime precipitation process (at pH 11.5) could be reduced from 220 to 100 hours to reach pH 8, using an aeration tank (A/V ratio of 5 m^2/m^3) with atmospheric air injection at 85 L h^{-1} during carbonation. In fact, the injection of air [51] or the turbulence of the water surface [52] can increase the gas-liquid interface and promote carbonation reactions. However, the increase in CO_2 flux is not linear with the reduction in carbonation time. Liendo et al. [5] observed that increasing the CO_2 flux from 100 to 1450 mL min^{-1} (at 99.9% purity) could reduce the neutralization time from 3 to 1.5 minutes, to reach pH 8. The problem with high flue gas CO_2 flows is the release of CO_2 into the environment, as some of it is not absorbed by the water [15]. In the case of atmospheric CO_2, this concern does not arise, as the atmospheric CO_2 that leaves the bubbling or capillary processes can be equal to or lower than what already existed in the atmosphere, but unnecessary energy expenditure is at stake.

Model component *D* seems to contribute to the increase of all response variables (Table S4), which according to ANOVA results (Table S6) has significant effects ($P<0.05$). As observed in Fig. 2a1–e1, all response variables increase with increasing SWW volume (curve D, from 178 to 478 mL), indicating that higher volumes of SWW impact the carbonation process. In fact, the greater the SWW volume to be treated, the greater the amount of atmospheric CO_2 necessary to neutralize the effluent [20]. Madeira et al. [20] also observed that the application of low reactor area/volume ratios (i.e., larger SWW volumes for a fixed area) in the carbonation process contributed to a longer carbonation time.

Regarding the capillary process (Table S5), model component *A* seems to contribute to the increase in the response variables studied, unlike model components *B* and *C*, which seem to be responsible for its decrease. However, the ANOVA results (Table S7) show that only the variables SWW flow rate (*A*), and capillary area (*C*) had significant effects ($P<0.05$) on pH, conductivity, calcium, total alkalinity, and ammonium nitrogen. According to Fig. 2a2–e2, all response variables increased with an increase in the SWW flow rate (curve *A*, from 1.2 to 2.0 mL min^{-1}). In fact, high SWW flow rates imply greater volumes of water to be treated per unit of time, which implies shorter water-air contact times in the system and consequently incomplete carbonation or even non-carbonatation. On the other hand, in the opposite direction, an increase in the capillary area (curve *C*, from 150 to 700 cm^2) contributed to the decrease in pH, conductivity, calcium, total alkalinity, and ammonium nitrogen (Fig. 2a2–e2). This means that the carbonation process can be compromised if there is not enough contact time between air and SWW, either by controlling the SWW flow rate and/or by the capillary area. In this work, the capillary area was the independent variable that had the greatest influence on response variables, given its clear sharp curve (Fig. 2a2–e2). Trus et al. [44] evaluated the effect of the area of the capillary material on the iron ions removal from water. These authors observed that the transition of Fe^{2+} to Fe^{3+} significantly depends on the contact area of water solution with air, and the reduction of the total iron content is directly proportional to the contact area.

Table 4
Regression equations for different parameters, in the bubbling and capillary processes.

Parameters	Equations Bubbling process	Capillary process
pH	$Y_1 = 11.14–1.12A - 0.0439B - 0.2028C + 0.7467D - 0.0950AB - 0.1562AC + 0.6713AD + 0.0413BC - 0.0312BD - 0.0825CD - 0.4551A^2 + 0.1249B^2 + 0.4049C^2 - 0.5101D^2$	$Y_6 = 9.70 + 0.2903A - 0.0259B - 1.61C - 0.0016AB + 0.1651AC - 0.0334BC + 0.1657A^2 - 0.4473B^2 + 0.8432C^2$
Conductivity (mS cm^{-1})	$Y_2 = 2.49–1.23A - 0.0652B - 0.3554C + 0.3542D - 0.1690AB - 0.0849AC - 0.0240AD + 0.2010BC - 0.0989BD - 0.2015CD + 0.4590A^2 - 0.0490B^2 + 0.5860C^2 - 0.2640D^2$	$Y_7 = 1.43 + 0.1271A - 0.0692B - 0.7802C - 0.0635AB - 0.1885AC + 0.0940BC - 0.0656A^2 + 0.0959B^2 + 0.9409C^2$
Calcium (mg L^{-1})	$Y_3 = 275.93–154.48A - 12.91B - 49.32C + 41.79D - 10.56AB - 15.77AC + 4.98AD + 27.67BC - 11.90BD - 17.44CD + 55.83A^2 + 22.78B^2 + 66.37C^2 - 52.19D^2$	$Y_8 = 110.29 + 11.27A - 1.61B - 86.38C + 6.04AB - 12.74AC + 12.74BC - 1.36A^2 - 6.72B^2 + 84.49C^2$
Total alkalinity (mg $CaCO_3$ L^{-1})	$Y_4 = 239.59–386.29A - 64.56B - 103.18C + 146.86D - 32.77AB - 33.14AC - 7.80AD + 67.24BC - 31.47BD - 73.21CD + 188.11A^2 + 73.82B^2 + 181.19C^2 - 79.34D^2$	$Y_9 = 221.49 + 50.65A - 9.42B - 180.21C - 11.78AB - 70.67AC + 26.50BC + 2.25A^2 - 27.20B^2 + 178.93C^2$
Ammonium (mg N L^{-1})	$Y_5 = 51.07–17.77A - 3.65B - 4.79C + 8.82D - 2.33AB - 2.66AC + 2.66AD + 1.96BC + 0.3525BD - 1.30CD + 4.35A^2 - 3.75B^2 + 15.61C^2 - 7.49D^2$	$Y_{10} = 25.21 + 2.48A - 0.3577B - 4.77C - 0.3554AB - 4.71AC + 1.70BC + 4.89A^2 - 3.01B^2 + 3.36C^2$

Note: A: Time; B: Air flow rate; C: Stirring speed; D: SWW volume, for the bubbling process. A: SWW flow rate; B: Air flow rate; C: Capillary area for the capillary process.

3.3.2. Interactive effects

Model components *AB*, *AC*, *AD*, *BC*, *BD,* and *CD* for the bubbling process and *AB*, *AC*, and *BC* for the capillary process represent the interaction between two independent variables, while A^2, B^2, C^2, and D^2 for bubbling process, and A^2, B^2, C^2 for capillary process represent their quadratic effects. Of all model components of the bubbling process, only the *AB* (for conductivity), *AC* (for pH, calcium, and ammonium), *AD* (for pH and ammonium), *BC* (for conductivity, calcium, and total alkalinity), *CD* (for conductivity, calcium, and total alkalinity), A^2 (for pH, conductivity, calcium, and total alkalinity), C^2 (for pH, conductivity, calcium, total alkalinity, and ammonium), D^2 (for pH, calcium, total alkalinity, and ammonium) components had significant combined

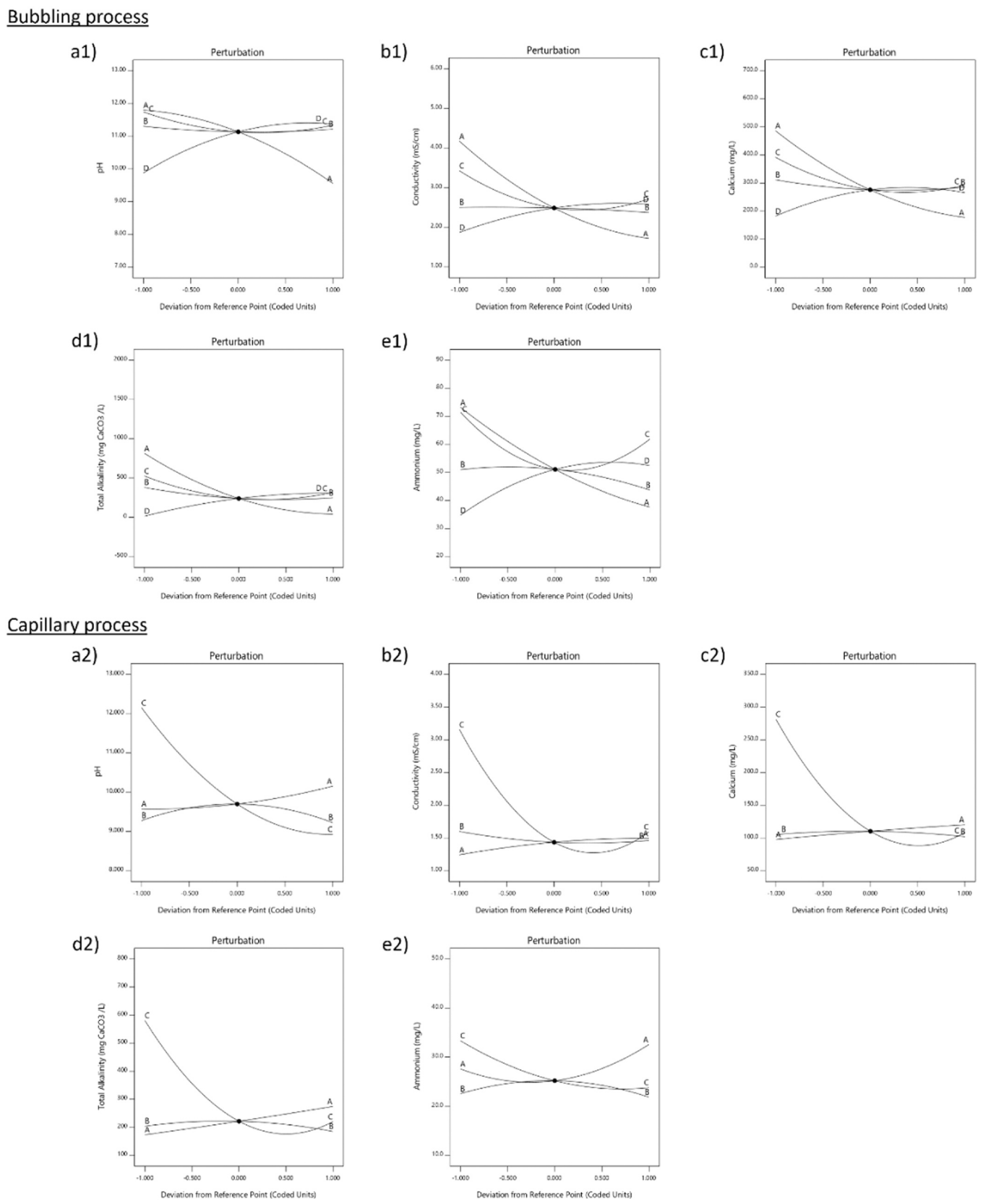

Fig. 2. Perturbation plot showing the effect of all independent variables on the: a) pH, b) conductivity, c) calcium, d) total alkalinity, and e) ammonium nitrogen. Numbers **1** and **2** refer to the bubbling process and the capillary process, respectively. Capital letters inside the figures represent the following independent variables: A - Time, B - Air flow rate, C - Stirring speed and D - SWW volume, for bubbling process, and A - SWW flow rate, B - Air flow rate and C - Capillary area, for capillary process.

effects ($P<0.05$), according to ANOVA results (Fig. S6). Among all these components, only the components *AB* (for conductivity), *AC* (for pH, calcium, and ammonium), *CD* (conductivity, calcium, and total alkalinity), A^2 (for pH) and D^2 (for pH, calcium, total alkalinity, and ammonium), contribute to the reduction of the respective response variables (Table S4). The response surface graphs show the different combined effects (Figs. 3–7). The combined effect time and stirring speed (*AC*) (at 90 L h^{-1} of air flow rate and 328 mL of SWW volume) on pH, calcium, and ammonium nitrogen (Figs. 3b, 5b, and 7b, respectively), show a greater decrease in pH, calcium, and ammonium nitrogen when the time was increased from 2 to 21 h, and the stirring speed was increased from 0 to 100–200 rpm. According to the combined effect of time and air flow rate (*AB*) (at 100 rpm of stirring speed and 328 mL of SWW volume) shown in Fig. 4a, lower conductivity values were achieved with increasing time from 0 to 21 h and increasing air flow rate from 60 to 120 L h^{-1}. On the other hand, the minimum pH and ammonium nitrogen values were reached when the combined effect of time and SWW volume (*AD*) (at 90 L h^{-1} of air flow rate and 100 rpm of stirring speed) occurred (Figs. 3c and 7c, respectively), that is, when the time was increased from 0 to 21 h and the SWW volume was reduced from 478 to 178 mL. Low values of conductivity, calcium, and total alkalinity were also observed for the combined effects of air flow rate and stirring speed (*BC*) (at 11.5 h of time and 328 mL of SWW volume) in the range of 60–120 L h^{-1} and 75–175 rpm (Figs. 4d, 5d, and 6d, respectively), as well as for stirring speed and SWW volume (*CD*) (at 11.5 h of time and 90 L h^{-1} of air flow rate) in the range 50–150 rpm and 178–238 mL (Figs. 4f, 5f and 6f, respectively).

For capillary process, the model components such as *AC* (for pH,

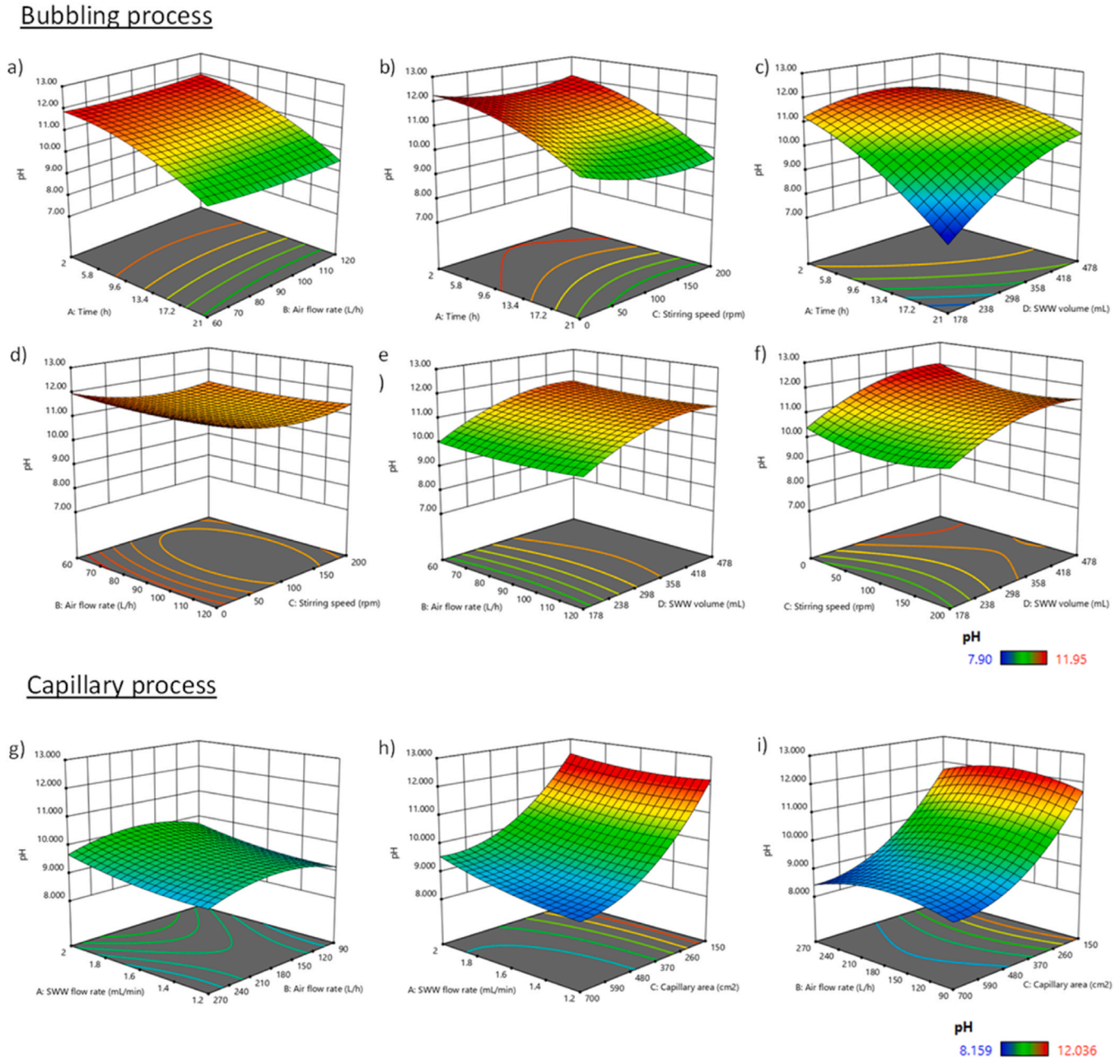

Fig. 3. Three-dimensional response surface graphs and contour plots of the pH, showing the effect of two variables (while the other variables are held at center level): a) time and air flow rate; b) time and stirring speed; c) time and SWW volume; d) air flow rate and stirring speed; e) air flow rate and SWW volume; and f) stirring speed and SWW volume, for the bubbling process, as well as g) SWW flow rate and air flow rate; h) SWW flow rate and capillary area; and i) air flow rate and capillary area, for capillary process.

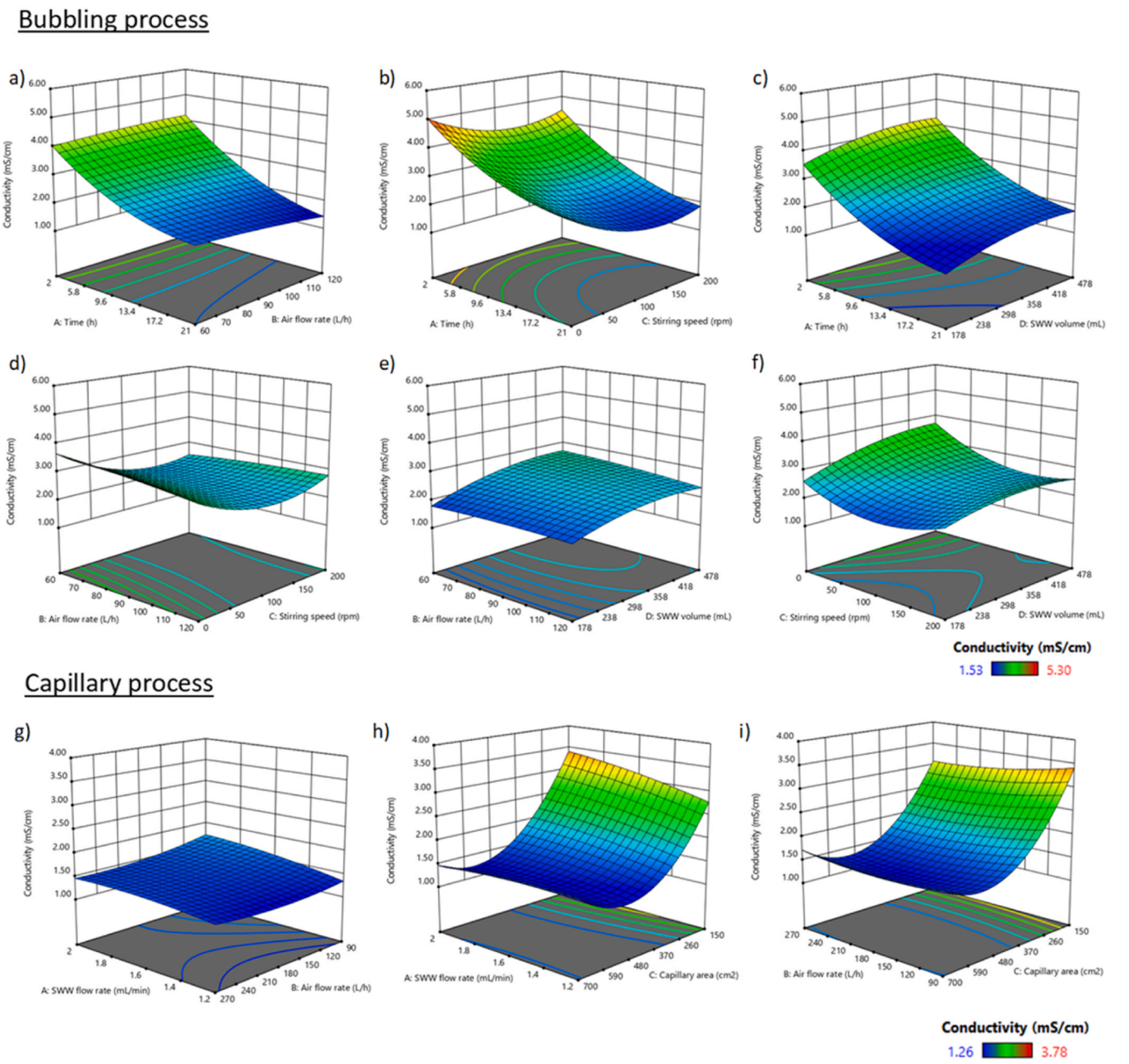

Fig. 4. Three-dimensional response surface graphs and contour plots of the conductivity, showing the effect of two variables (while the other variables are held at center level): a) time and air flow rate; b) time and stirring speed; c) time and SWW volume; d) air flow rate and stirring speed; e) air flow rate and SWW volume; and f) stirring speed and SWW volume, for the bubbling process, as well as g) SWW flow rate and air flow rate; h) SWW flow rate and capillary area; and i) air flow rate and capillary area, for capillary process.

conductivity, calcium, total alkalinity, and ammonium), *BC* (for calcium and ammonium), A^2 (for ammonium), B^2 (for pH and ammonium), C^2 (for pH, conductivity, calcium, total alkalinity, and ammonium), had a significant combined effect ($P<0.05$) on the respective response variables, according to ANOVA results (Table S7). Only the components *AC* (for conductivity, calcium, total alkalinity, and ammonium) and B^2 (for pH and ammonium) are responsible for the reduction of the respective response variables (Table S5). For combined effect of SWW flow rate and capillary area (*AC*) (at 180 L h^{-1} of air flow rate) (Figs. 3h, 4h, 5h, 6h, and 7h), all response variables had their minimum values when the capillary area increased from 150 to 700 cm^2, and the SWW flow rate was between 1.2 and 2.0 mL min^{-1} (although for pH (Fig. 3h) and ammonium nitrogen (Fig. 7h) it was preferable to reach low and high values of this range, respectively).

According to Viswanaathan et al. [31], the rate of dissolution of atmospheric CO_2 in water depends on factors, such as contact time, area at the gas-liquid interface, concentration of CO_2 in the atmosphere, and solution properties (including pH, temperature, concentration of dissolved salts, and others). This dissolution can be enhanced if all these factors are considered. The decrease in pH, calcium, conductivity, and total alkalinity that was observed in both processes is related to carbonation reactions with atmospheric CO_2 (Eqs.2 to 5), as occurs in the ocean acidification process [53–55].

$$CO_2\ (g) \rightleftarrows CO_2\ (aq) \quad (2)$$

$$CO_2\ (aq) + H_2O\ (l) \rightleftarrows H_2CO_3\ (aq) \quad (3)$$

$$H_2CO_3 \rightleftarrows H^+ + HCO_3^- \quad (4)$$

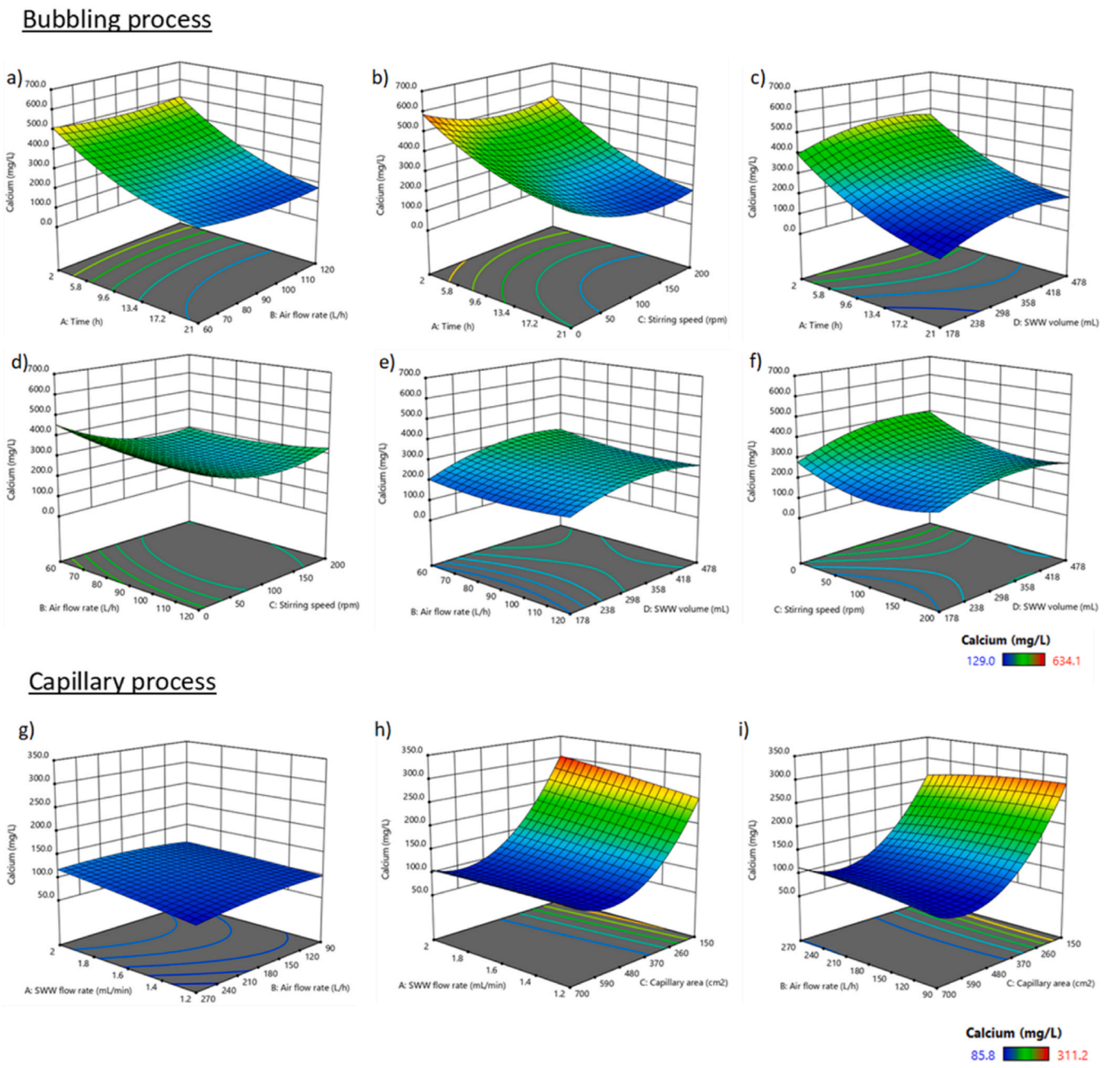

Fig. 5. Three-dimensional response surface graphs and contour plots of the calcium, showing the effect of two variables (while the other variables are held at center level): a) time and air flow rate; b) time and stirring speed; c) time and SWW volume; d) air flow rate and stirring speed; e) air flow rate and SWW volume; and f) stirring speed and SWW volume, for the bubbling process, as well as g) SWW flow rate and air flow rate; h) SWW flow rate and capillary area; and i) air flow rate and capillary area, for capillary process.

$$HCO_3^- \rightleftarrows H^+ + CO_3^{2-} \quad (5)$$

$$CO_3^{2-} + Ca^{2+} \rightleftarrows CaCO_3 \quad (6)$$

Free CO_2 is not available in the pretreated SWW by IOSLM at pH 12, which causes a chemical imbalance of CO_2 between the water and the air inside the reactor of both processes. As a way of counteracting this imbalance, the CO_2 present inside the reactor tends to dissolve in water through the water-air interface until reaching equilibrium (Eq. 2). After dissolution in water, the dissolved CO_2 is subjected to a hydration reaction by reacting with water to form H_2CO_3 (Eq. 3). As H_2CO_3 is a weak acid, it dissociates in two steps, the first step (Eq. 4) being the formation of HCO_3^- and H^+ ions, and the second step (Eq. 5) the formation of CO_3^{2-} and ions H^+, from HCO_3^-. The production of H^+ ions leads to a decrease in the pH of the effluent. In turn, the carbonate ions react with the calcium ions present in the water, forming the precipitated calcium carbonate (Eq. 6) [56]. Consequently, the conductivity may decrease with the removal of calcium. In fact, in this work, high correlations ($r = 0.98$, $P<0.05$, Tables S8 and S9) were found between calcium and conductivity, in both processes. During the carbonation process, alkalinity is consumed due to the reaction with hydroxide ions and ammonium nitrogen removal [29,39]. The decrease in ammonium nitrogen in the water is due to the volatilization of ammonia at pH > 9.2, since at high pH most of the ammoniacal nitrogen is in the form of ammonia which can be volatilized. As the pH decreases, ammonia will tend to be in equilibrium with the ammonium ion (Eq. 7), and its removal will be

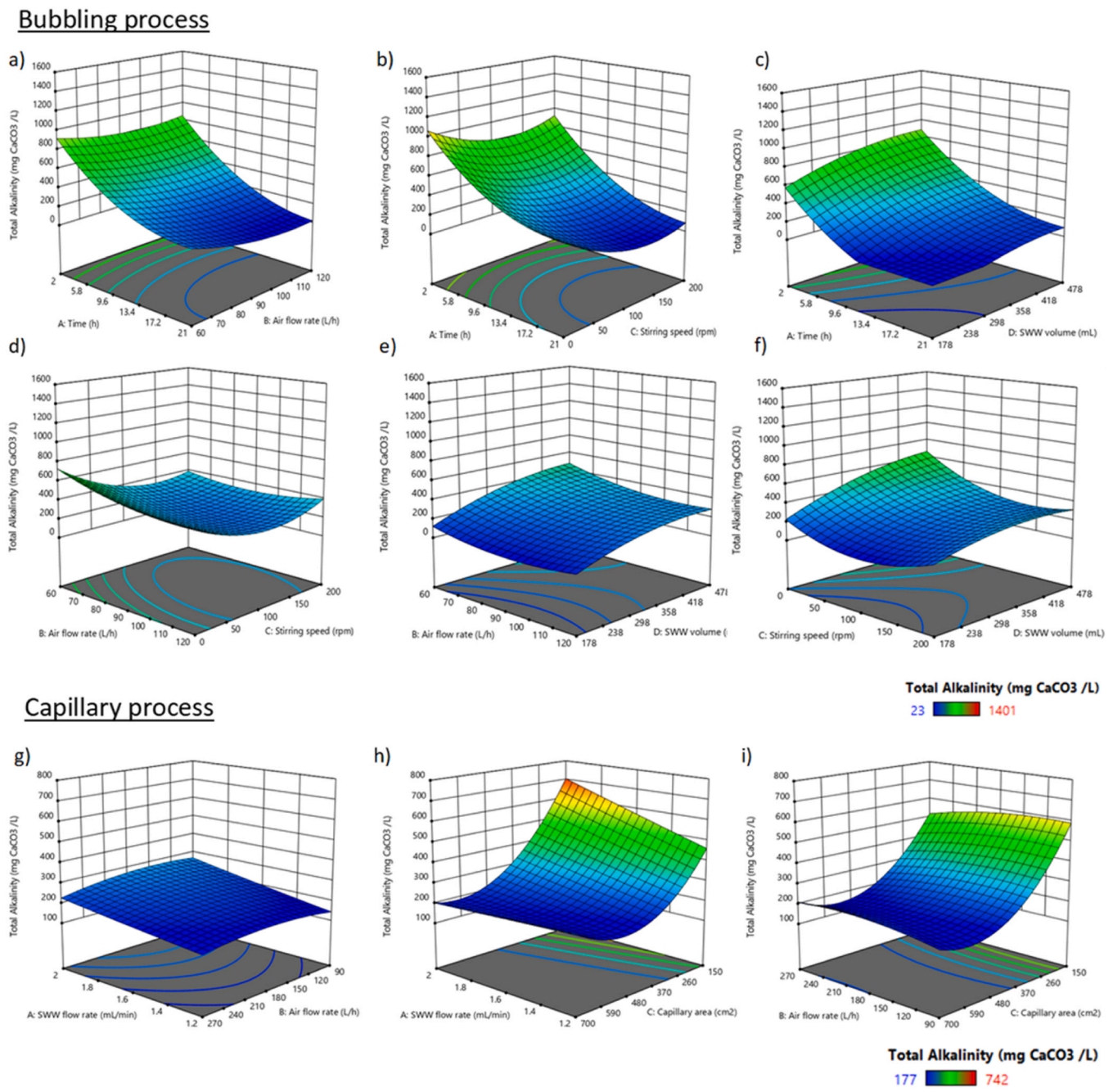

Fig. 6. Three-dimensional response surface graphs and contour plots of the total alkalinity, showing the effect of two variables (while the other variables are held at center level): a) time and air flow rate; b) time and stirring speed; c) time and SWW volume; d) air flow rate and stirring speed; e) air flow rate and SWW volume; and f) stirring speed and SWW volume, for the bubbling process, as well as g) SWW flow rate and air flow rate; h) SWW flow rate and capillary area; and i) air flow rate and capillary area, for capillary process.

more difficult [57].

$$NH_4^+ + OH^- \rightarrow H_2O + NH_3 \quad (7)$$

3.4. Optimization of operating conditions

The goals, the upper and lower limits, and the importance intended for each of the independent and response variables for numerical optimization are described in Tables S10 and S11, for the bubbling and the capillary processes, respectively. Thus, considering the restrictions presented, about 56 optimal solutions (Table S12) for the bubbling process and 22 optimal solutions (Table S13) for the capillary process were found, respectively. For the bubbling process, the optimal solution selected was the one that had the greatest desirability, that is, 0.830 with the following characteristics of the response variables (pH (8.0), conductivity (1.527 mS cm^{-1}), calcium (152.1 mg L^{-1}, corresponding a 76% of removal), total alkalinity (25.4 mg $CaCO_3$ L^{-1}) and ammonium (28.6 mg N-NH_4^+ L^{-1}, corresponding a 66.2% of removal)) and independent variables (time (21 h), air flow rate (65 L h^{-1}), stirring speed (52 rpm) and SWW volume (178 mL)) (Table S12). For the capillary process, with desirability of 0.858, the selected optimal solution found the following values of pH (8.2), conductivity (1.599 mS cm^{-1}), calcium (96.7 mg L^{-1}, corresponding a 81.0% of removal), total alkalinity

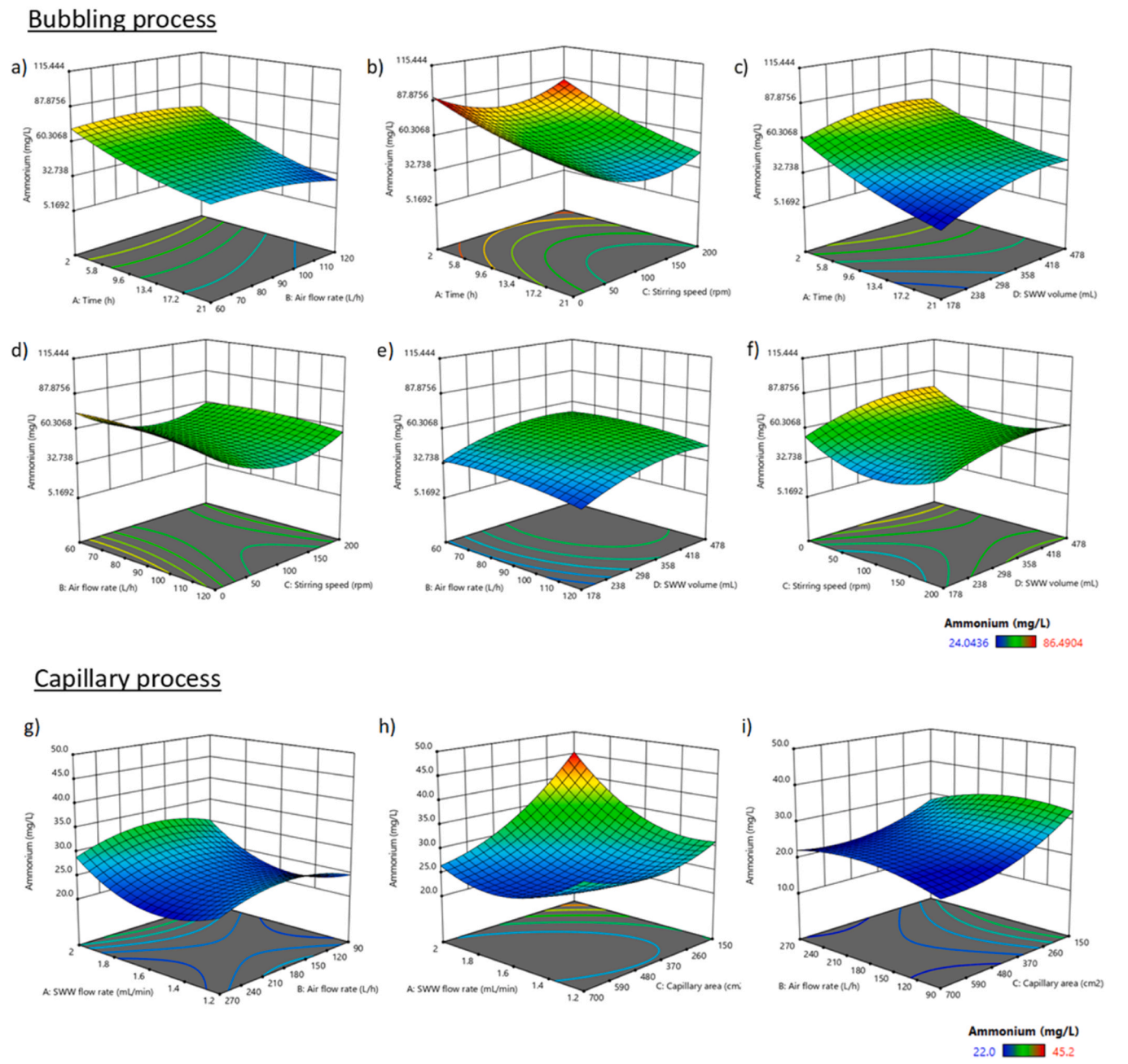

Fig. 7. Three-dimensional response surface graphs and contour plots of the ammonium nitrogen, showing the effect of two variables (while the other variables are held at center level): a) time and air flow rate; b) time and stirring speed; c) time and SWW volume; d) air flow rate and stirring speed; e) air flow rate and SWW volume; and f) stirring speed and SWW volume, for the bubbling process, as well as g) SWW flow rate and air flow rate; h) SWW flow rate and capillary area; and i) air flow rate and capillary area, for capillary process.

(186 mg $CaCO_3$ L^{-1}), and ammonium (26.2 mg N-NH_4^+ L^{-1}, corresponding a 57.5% of removal), associated with the values of the independent variables: SWW flow rate (1.2 mL min^{-1}), air flow rate (90 L h^{-1}) and capillary area (700 cm^2) (Table S13).

On the other hand, the optimization process was also complemented with graphic optimization using the constraints of the previously defined response variables (Tables S10 and S11) and the values of the independent variables of the previously selected optimal solutions (Tables S12 and S13), as can be seen in Fig. 8 (for the bubbling process) and 9 (for the capillary process). In fact, the graphical optimization results allow a faster search for the ideal settings for the occurrence of atmospheric carbonation, where the colored areas on the graphical optimization plot indicate the region of interest, while the regions do not meet the proposed criteria are shaded out. According to the graphic optimization shown in Fig. 8 (for the bubbling process), all the colored regions were limited by the time from 19.5 to 21 h, simultaneously with the following independent variables: air flow rate between 60 and 65 L h^{-1} (under stirring speed at 52 rpm and SWW volume of 178 mL) (Fig. 8a), stirring speed between 0 and 55 rpm (under an air flow rate of 65 L h^{-1} and SWW volume of 178 mL) (Fig. 8b) and SWW volume between 178 and 215 mL (under air flow rate at 65 L h^{-1} and stirring speed at 52 rpm) (Fig. 8c). In fact, time seems to be the determining factor in the bubbling process, requiring about 19–21 hours for atmospheric carbonation to be achieved. As can be seen in Fig. 8d, the colored region can be reached with an air flow rate of around 67–103 L h^{-1} and stirring speed of around 8–54 rpm, if the time of 21 h and SWW volume

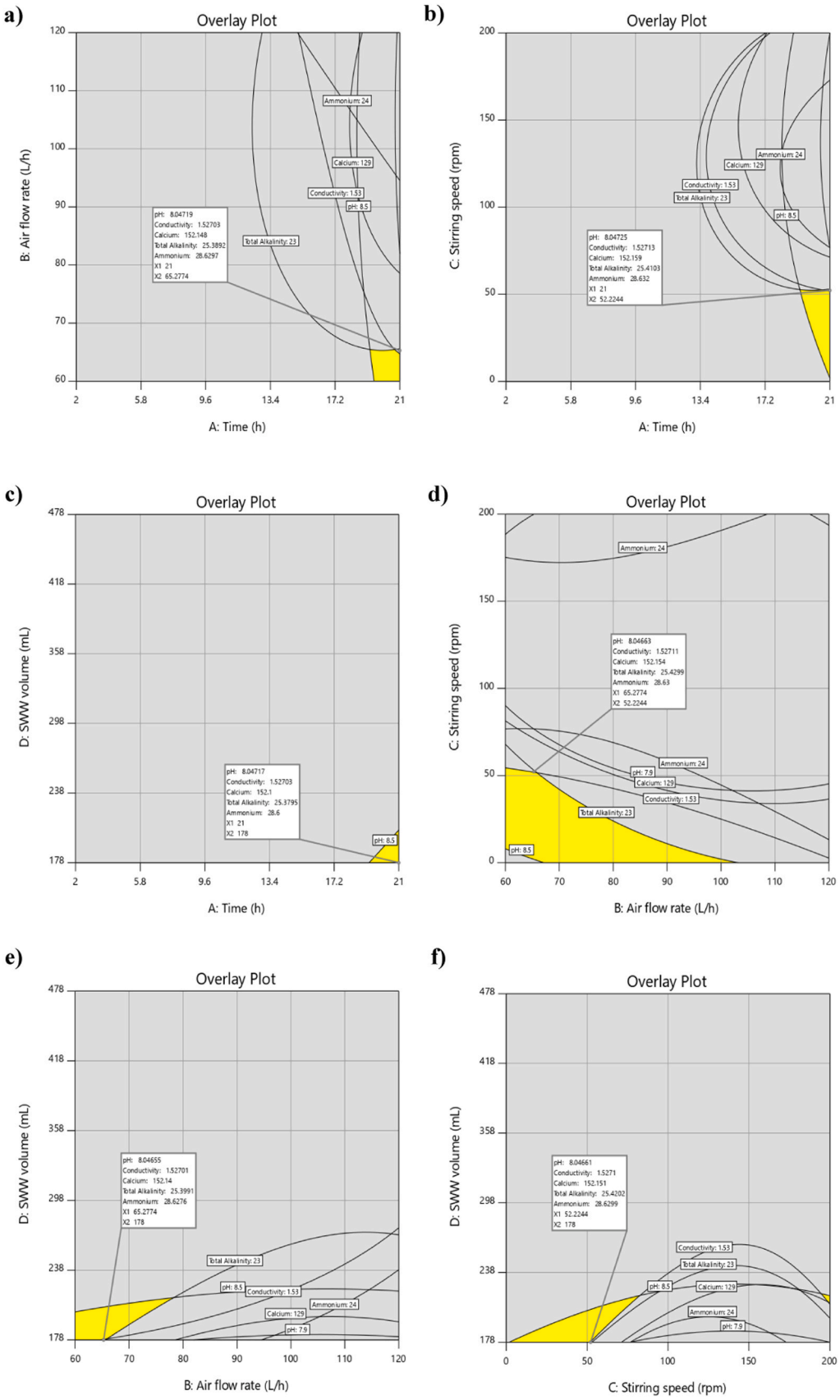

Fig. 8. Overlay plot for optimal region based on the criterion defined for the bubbling process, namely: a) time versus air flow rate at stirring speed of 52 rpm and SWW volume of 178 mL; b) time versus stirring speed at air flow rate of 65 L h^{-1} and SWW volume of 178 mL; c) time versus SWW volume at air flow rate of 65 L h^{-1} and stirring speed of 52 rpm; d) air flow rate versus stirring speed at time of 21 h and SWW volume of 178 mL; e) air flow rate versus SWW volume at time of 21 h and stirring speed of 52 rpm; and f) stirring speed versus SWW volume at time of 21 h and air flow rate of 65 L h^{-1}.

of 178 mL were considered. However, in terms of energy costs, it may be preferable to apply only an air flow rate of 67 L h^{-1} without agitation. On the other hand, according to Fig. 8e and f, the SWW volume can be increased from 178 mL to 214 and 216 mL, respectively, if, in the first case, the air flow rate is increased to 77 L h^{-1} (keeping constant time to 21 h and stirring speed to 52 rpm) or in the second case, stirring speed is increased to 82 rpm (keeping constant time to 21 h and air flow rate to 65 L h^{-1}).

For the capillary process, Fig. 9a and c showed two distinct colored regions. One of the regions is limited by the low values of air flow rate (about 90–123 L h^{-1}) when they are applied simultaneously with low values of SWW flow rate (about 1.20–1.41) under capillary area at 700 cm^2 (Fig. 9a), or high capillary area values (657–700 cm^2) under constant SWW flow rate at 1.2 mL min^{-1} (Fig. 9c). The other region is limited by the high values of air flow rate (224–270 L h^{-1}) when they are applied together with low values of SWW flow rate (1.2–1.64 mL min^{-1}) under capillary constant area at 700 cm^2 (Fig. 9a), or high capillary area values (619–700 cm^2) under constant SWW flow rate at 1.2 mL min^{-1} (Fig. 9c). Although the SWW flow rate range of 1.2–1.64 mL min^{-1} can be achieved in the colored region (Fig. 9a), the results indicated that 1.2 and 1.6 mL min^{-1} corresponded to the minimum and maximum of the defined pH range 8.2–8.5, respectively. In fact, as noted above, the increase in the SWW flow rate contributed to the increase in the effluent pH. In terms of energy costs, it is preferable to choose the region with low air flow rate values. Moreover, for both processes studied, the identification of optimal regions at low air flow rates, indicates that the air flows used were not too low to prevent a restoration of atmospheric CO_2 in the system and consequently limit the atmospheric carbonation process. Concerning Fig. 9b, the colored region is limited by high capillary area values (687–700 cm^2) and low SWW

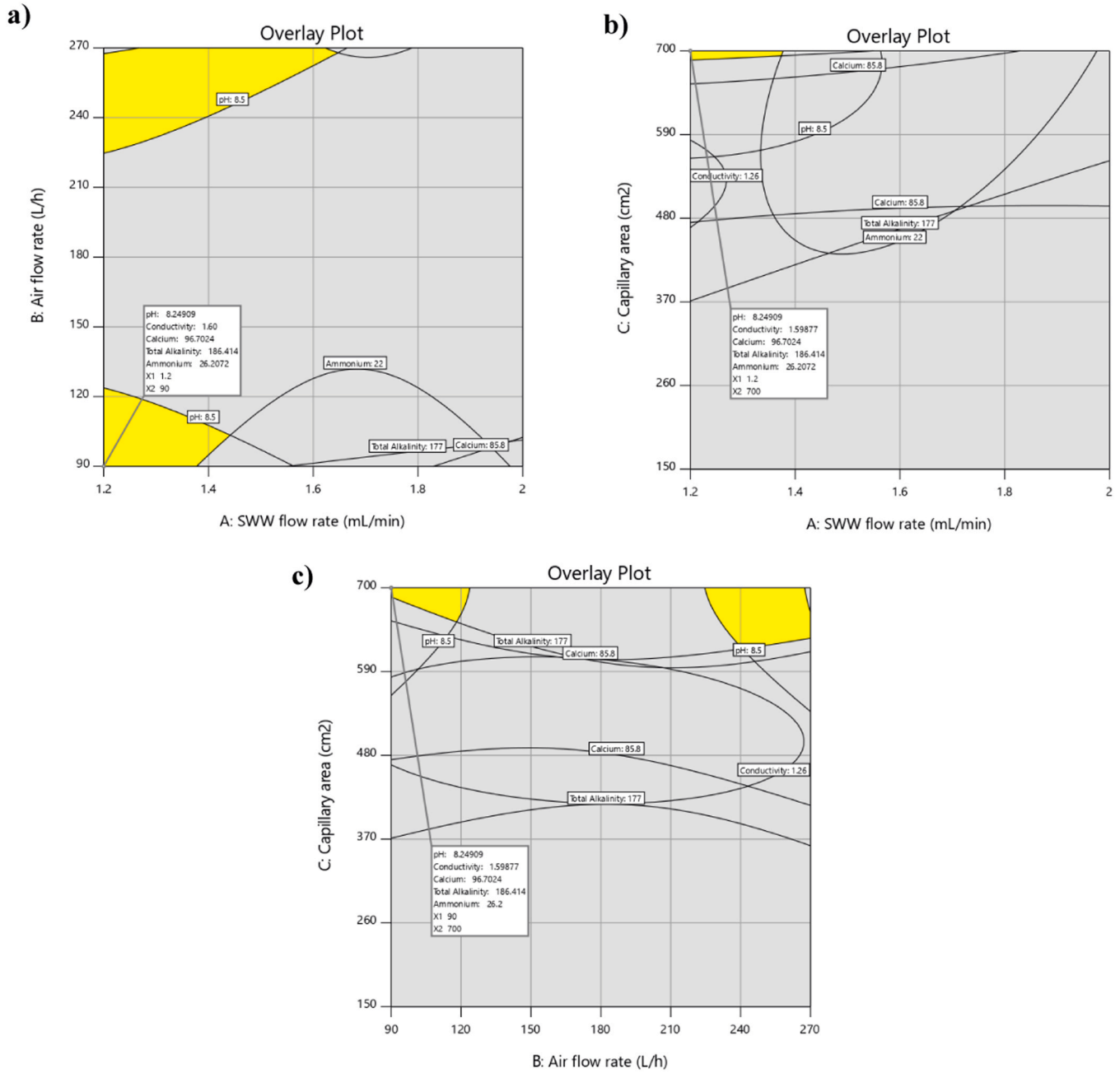

Fig. 9. Overlay plot for optimal region based on the criterion defined for the capillary process, namely: a) SWW flow rate versus air flow rate at capillary area of 700 cm^2; b) SWW flow rate versus capillary area at air flow rate of 90 L h^{-1}; and c) air flow rate versus capillary area at SWW flow rate of 1.2 mL min^{-1}.

flow rates (1.2–1.38 mL min^{-1}), when an air flow rate of 90 L h^{-1} is applied.

3.5. Validation of the optimal conditions

Table 5 shows the validation of the optimal conditions for the bubbling process (using time of 21 h, air flow rate of 90 L h^{-1}, no stirring speed, and SWW volume of 178 mL, as can be seen in Fig. 8) and capillary process (using SWW flow rate of 1.2 mL min^{-1}, air flow rate of 90 L h^{-1} and capillary area of 700 cm^2, in Fig. 9). According to Table 5, the differences between the actual values and the predicted values were small, in all the response variables, for both processes, which means that the developed models can predict the response variables with significant accuracy. For the bubbling process and the capillary process, the ammonium nitrogen capture under these operating conditions was about 99±2%. Thus, it can be said that these processes, compared to atmospheric carbonation processes in open systems, can contribute to the capture and recovery of ammonium nitrogen.

The effectiveness of the capillary process to treat different SWW volumes (178–478 mL) under the previously found optimal condition was investigated (Fig. 10). The time required to collect the pretreated SWW volumes of 178, 328, and 478 mL was 4.48, 7.38, and 10.20 hours, respectively. According to Fig. 10, there were no significant ($P<0.05$) differences in the values of pH (Fig. 10a), conductivity (Fig. 10b), calcium (Fig. 10c), total alkalinity (Fig. 10d), and ammonium nitrogen (Fig. 10e), for the different volumes collected (i.e., 178, 328, and 478 mL). Therefore, regardless of the volume collected, calcium, and ammonium removals were around 82.6 and 57.2%, respectively, with a substantial reduction in pH to 8.2 and conductivity to 1.5 mS cm^{-1}. These results indicate that, unlike the batch bubbling process which was only effective for SWW volumes around 178 mL (Fig. 8c, e, and f), the capillary process can treat the effluent continuously and dispose of the effluent immediately for the following treatment processes. Furthermore, the capillary process proved to be more efficient than the bubbling process, requiring about 4.48 h to reduce the pH to around 8 for 178 mL of SWW, while the bubbling process would take 19–21 h and result in greater energy expenditure by the air pump. In capillary process, the movement of water within the spaces of a porous material, occurs without energy due to the forces of adhesion, cohesion, and surface tension. Moreover, the bubbling process still requires a settling time to remove the calcium carbonate precipitate from the solution, which does not happen in the capillary process whose collected effluent was clean. Anyway, the static atmospheric carbonation processes found in the literature [29,37–39,50] seem to be less efficient than both processes studied, in which the former have long carbonation times ($\geq$ 7 days) to reach pH 8. In fact, the contact areas between air and water are greater in processes studied than in static atmospheric carbonation processes. In the bubbling process occurs the creation of water splashing in the air. On the other hand, in the capillary process the distribution of water along the entire length of the capillary, whose area of contact between the air and water is twice the capillary area since the capillary, can be wet either at the top or at the bottom. In static atmospheric carbonation processes, the water is at rest and the area of contact between the air and the water is just the surface area of the reactor [40]. However, when the neutralization of effluent is reached, it is observed that the ammonium nitrogen removal in the bubbling process (about 54.4% according to results from Tables 1 and 5) or in the capillary process (about 56.2% according to results from Tables 1 and 5) seems to be less efficient than the static and open atmospheric carbonation processes found in the literature. For example, the authors Madeira et al. [20], Ramalho et al. [39] and Madeira et al. [29] obtained 68.1–82.6%, 100% and 61.6% ammonium removals, respectively, when they studied atmospheric carbonation in open system. In fact, in the former, there is a possibility of the volatilized ammonia being mixed again with water, given the turbulence of the water or air in the reactors. Reducing the pH to around neutrality with simultaneous low nitrogen removal in the processes studied favors the production of nitrogen-rich effluents that could be used by plants. Calcium removals were higher than those observed in most cases studied (around 70.5% and 82.1% for bubbling and capillary processes, respectively, according to results from Tables 1 and 5) [20,29,37,38,39,50].

4. Conclusion

The purpose of this study was to evaluate the neutralization of slaughterhouse wastewaters treated by lime precipitation, by capturing atmospheric CO_2 in the lab-scale stirrer bubble column and lab-scale stepped continuous flow capillary column. Response surface methodology was used to model and optimize the lab-scale stirrer bubble and lab-scale stepped continuous flow capillary columns. Both processes were able to neutralize the lime precipitation treated slaughterhouse effluent. The optimal conditions to reach pH 8 in the bubbling process were 21 h, air flow rate at 65 L h^{-1}, stirring speed at 52 rpm, and SWW volume at 178 mL, and removals of 76.0% of calcium and 66.2% of ammonium nitrogen were obtained. In the bubbling process, the agitation step can be removed if higher air flow rate is applied, which can consequently reduce the associated energy costs. For the capillary process, the optimal conditions to reach pH 8.2 were SWW flow rate at 1.2 mL min^{-1}, air flow rate at 90 L h^{-1}, and capillary area at 700 cm^2, and removals of 81.0% calcium and 57.5% ammonium nitrogen were observed. Both processes proved to be more efficient compared to carbonation processes carried out in static reactors since significantly shorter carbonation times were obtained. Compared to the bubbling process, the capillary process was more efficient in neutralizing the effluent, contributing to a faster drop in pH, without the need for prior sedimentation to remove the precipitated $CaCO_3$ and greater energy consumption. Both processes provide a low-cost and eco-friendly alternative neutralization of alkaline wastewaters, with the recovery of volatilized ammonia during the carbonation process and without loss of ammonia to the atmosphere, in addition to a substantial removal of calcium.

The next works to be carried out should:

- Focus on the recovery of calcium carbonate present in the capillary, given that this product has potential value in several industries.

Table 5
Results of the model validation for the bubbling process and the capillary processes, using optimal conditions.

Variables	Bubbling process[a])			Capillary process[b])		
	Predicted value	Actual value[c])	Error (%)	Predicted value	Actual value[c])	Error (%)
pH	8.31	8.26	0.61	8.25	8.30	0.60
Conductivity (mS cm^{-1})	1.95	1.91	2.09	1.60	1.57	1.91
Calcium (mg L^{-1})	192.3	187	2.83	96.7	91.2	6.03
Total alkalinity (mg $CaCO_3$ L^{-1})	67	74	9.46	186	206	9.71
Ammonium (mg N-NH_4^+ L^{-1})	40.4	38.5	4.94	26.2	27.0	2.96

Note: a) Optimal conditions: $A = 21$ h, $B = 90$ L/h, $C = 0$ rpm, and $D = 178$ mL; b) Optimal conditions: $A = 1.2$ mL min^{-1}, $B = 90$ L/h, and $C = 700$ cm^2; c) N = 3. The experimental values obtained are part of the 95% confidence interval.

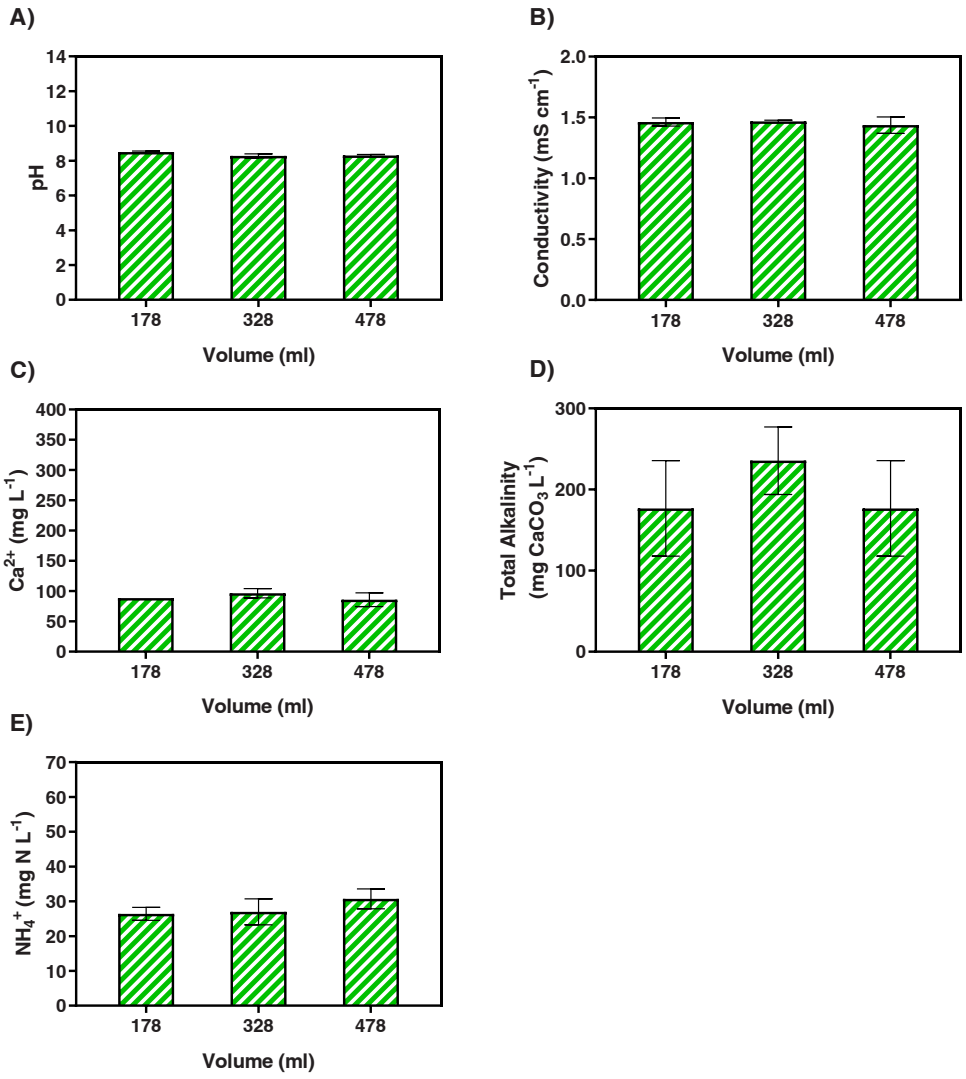

Fig. 10. Water quality analyzed in terms of: a) pH; b) conductivity; c) calcium; d) total alkalinity; and e) ammonium nitrogen, at different SWW volumes collected (178–478 mL), applying the optimal conditions of the capillary process (SWW flow rate at 1.2 mL min^{-1}, air flow rate at 90 L/h, and capillary area at 700 cm^2). Bars represent standard deviation of the mean.

- Evaluate the effect of temperature and CO_2-laden environments (for example, CO_2 resulting from the thermal treatment of sludge for reuse in the IOSLM process [6] on alkaline wastewater neutralization.

CRediT authorship contribution statement

Ribau Teixeira Margarida: Funding acquisition, Methodology, Supervision, Writing – review & editing. **Carvalho Fátima:** Conceptualization, Funding acquisition, Supervision, Writing – review & editing. **Madeira Luís:** Conceptualization, Investigation, Methodology, Writing – original draft.

Declaration of Competing Interest

The authors declare the following financial interests/personal relationships which may be considered as potential competing interests: Luis Madeira reports a relationship with Fundação para a Ciência e Tecnologia that includes: funding grants. Luis Madeira has patent #A process for treating wastewater using atmospheric CO2 pending to Instituto Politécnico de Beja.

Data availability

Data will be made available on request.

Acknowledgments

The authors thank the slaughterhouse for providing the effluent and help during effluent sample collection. We thank Professor Teresa Carvalhos (Polytechnic Institute of Beja), for providing the equipment to measure air quality. Luís Madeira also thanks FCT – Fundação para a Ciência e a Tecnologia for granting a PhD scholarship (SFRH/BD/137209/2018).

Appendix A. Supporting information

Supplementary data associated with this article can be found in the online version at doi:10.1016/j.jcou.2024.102705.

References

[1] A. Sattari, A. Ramazani, H. Aghahosseini, M.K. Aroua, The application of polymer containing materials in CO_2 capturing via absorption and adsorption methods, J. CO_2 Util. 48 (2021) 101526, https://doi.org/10.1016/J.JCOU.2021.101526.

[2] W.L. Tan, A.L. Ahmad, C.P. Leo, S.S. Lam, A critical review to bridge the gaps between carbon capture, storage and use of $CaCO_3$, J. CO_2 Util. 42 (2020) 101333, https://doi.org/10.1016/J.JCOU.2020.101333.

[3] K. Zhang, D. Guo, X. Wang, Y. Qin, L. Hu, Y. Zhang, R. Zou, S. Gao, Sustainable CO_2 management through integrated CO_2 capture and conversion, J. CO_2 Util. 72 (2023) 102493, https://doi.org/10.1016/J.JCOU.2023.102493.

[4] I. Ghiat, T. Al-Ansari, A review of carbon capture and utilisation as a CO_2 abatement opportunity within the EWF nexus, J. CO_2 Util. 45 (2021) 101432, https://doi.org/10.1016/J.JCOU.2020.101432.

[5] F. Liendo, M. Arduino, F.A. Deorsola, S. Bensaid, Optimization of $CaCO_3$ synthesis through the carbonation route in a packed bed reactor, Powder Technol. 377 (2021) 868–881, https://doi.org/10.1016/j.powtec.2020.09.036.

[6] H. Pashaei, A. Ghaemi, M. Nasiri, M. Heydarifard, Experimental investigation of the effect of nano heavy metal oxide particles in piperazine solution on CO_2 absorption using a stirrer bubble column, Energy Fuels 32 (2018) 2037–2052, https://doi.org/10.1021/ACS.ENERGYFUELS.7B03481.

[7] D.S. Cruz-Navarro, V. Mugica-Álvarez, M. Gutiérrez-Arzaluz, M. Torres-Rodríguez, CO_2 capture by alkaline carbonation as an alternative to a circular economy, Appl. Sci. 10 (2020) 863, https://doi.org/10.3390/APP10030863.

[8] I.R. Salmón, N. Cambier, P. Luis, CO_2 capture by alkaline solution for carbonate production: a comparison between a packed column and a membrane contactor, Appl. Sci. 8 (2018) 996, https://doi.org/10.3390/APP8060996.

[9] F. Azizi, L. Kaady, M. Al-Hindi, Chemical absorption of CO_2 in alkaline solutions using an intensified reactor, Can. J. Chem. Eng. 100 (2022) 2172–2190, https://doi.org/10.1002/CJCE.24420.

[10] E. Heidaryan, B. Aghel, S. Sahraie, M. Maleki, Enhanced carbon dioxide absorption using alcohol solvents in a microreactor: comparison with MEA + water mixture, J. Taiwan Inst. Chem. Eng. 151 (2023) 105105, https://doi.org/10.1016/J.JTICE.2023.105105.

[11] H. Pashaei, M.N. Zarandi, A. Ghaemi, Experimental study and modeling of CO_2 absorption into diethanolamine solutions using stirrer bubble column, Chem. Eng. Res. Des. 121 (2017) 32–43, https://doi.org/10.1016/J.CHERD.2017.03.001.

[12] E. Heidaryan, A. Gouran, K. Nejati, B. Aghel, Enhancement of CO_2 capture operation in oscillatory baffled reactor, Sep. Purif. Technol. 324 (2023) 124536, https://doi.org/10.1016/J.SEPPUR.2023.124536.

[13] B. Aghel, M. Maleki, S. Sahraie, E. Heidaryan, Desorption of carbon dioxide from a mixture of monoethanolamine with alcoholic solvents in a microreactor, Fuel 306 (2021) 121636, https://doi.org/10.1016/J.FUEL.2021.121636.

[14] M. Uibu, O. Velts, A. Trikkel, R. Kuusik, Reduction of CO_2 emissions by carbonation of alkaline wastewater, WIT Trans. Ecol. Environ. 116 (2008) 311–320, https://doi.org/10.2495/AIR080321.

[15] J. Yoo, H. Shin, S. Ji, An eco-friendly neutralization process by carbon mineralization for Ca-rich alkaline wastewater generated from concrete sludge, Metals 7 (2017) 371, https://doi.org/10.3390/MET7090371.

[16] A.A. Filimonova, N.D. Chichirova, A.A. Chichirov, A.I. Minibaev, R.V. Buskin, Processing of alkaline wastewater of TPP evaporative water treatment plant with electromembrane methods, IOP Conf. Ser. Earth Environ. Sci. 288 (2019) 012009, https://doi.org/10.1088/1755-1315/288/1/012009.

[17] D. Qi, Treatment of wastewater, off-gas, and waste solid. Hydrometallurgy of Rare Earths, Elsevier, 2018, pp. 743–777, https://doi.org/10.1016/b978-0-12-813920-2.00008-8.

[18] O. Velts, M. Uibu, J. Kallas, R. Kuusik, CO_2 mineralisation: concept for co-utilization of oil shale energetics waste streams in $CaCO_3$ production, Energy Procedia 37 (2013) 5921–5928, https://doi.org/10.1016/J.EGYPRO.2013.06.518.

[19] L. Madeira, A. Almeida, A.M.R. da Costa, A.S. Mestre, F. Carvalho, M.R. Teixeira, Tunning processes for organic matter removal from slaughterhouse wastewater treated by immediate one-step lime precipitation and atmospheric carbonation, J. Environ. Chem. Eng. 11 (2023) 110450, https://doi.org/10.1016/J.JECE.2023.110450.

[20] L. Madeira, F. Carvalho, A. Almeida, M. Ribau Teixeira, Optimization of atmospheric carbonation in the integrated treatment immediate one-step lime precipitation and atmospheric carbonation. The case study of slaughterhouse effluents, Results Eng. 17 (2023) 100807, https://doi.org/10.1016/j.rineng.2022.100807.

[21] L. Madeira, M. Ribau Teixeira, A. Almeida, T. Santos, F. Carvalho, Reuse of lime sludge from immediate one-step lime precipitation process as a coagulant (aid) in slaughterhouse wastewater treatment, J. Environ. Manag. 342 (2023) 118278, https://doi.org/10.1016/J.JENVMAN.2023.118278.

[22] A. Martínez-Cruz, A. Fernandes, F. Ramos, S. Soares, P. Correia, A. Baía, A. Lopes, F. Carvalho, An eco-innovative solution for reuse of leachate chemical precipitation sludge: application to sanitary landfill coverage, Ecol. Eng. Environ. Technol. 22 (2021) 52–58, https://doi.org/10.12912/27197050/133329.

[23] M. Mortula, T. Ali, A. Elaksher, Municipal wastewater treatment using different coagulants, Desalin. Water Treat. 179 (2020) 1–7, https://doi.org/10.5004/DWT.2020.24989.

[24] H. Prasad, R.K. Lohchab, B. Singh, A. Nain, M. Kumari, Lime treatment of wastewater in a plywood industry to achieve the zero liquid discharge, J. Clean. Prod. 240 (2019) 118176, https://doi.org/10.1016/J.JCLEPRO.2019.118176.

[25] A.R. Prazeres, S. Luz, F. Fernandes, E. Jerónimo, Cheese wastewater treatment by acid and basic precipitation: application of H_2SO_4, HNO_3, HCl, $Ca(OH)_2$ and NaOH, J. Environ. Chem. Eng. 8 (2020) 103556, https://doi.org/10.1016/J.JECE.2019.103556.

[26] R.K. Goel, J.R.V. Flora, J.P. Chen, Flow equalization and neutralization. Physicochemical Treatment Processes, Humana Press, 2005, pp. 21–45, https://doi.org/10.1385/1-59259-820-x:021.

[27] Y.-J. Park, H.-C. Lee, A study on the field application of alkaline tunnel wastewater to neutralization using CO_2, J. Korean Geotech. Soc. 36 (2020) 27–34, https://doi.org/10.7843/KGS.2020.36.8.27.

[28] D.Y. Kang, M.R. Kim, J.H. Lim, T.Y. Lee, J.K. Lee, Neutralization of alkaline wastewater with CO_2 in a continuous flow jet loop reactor, Korean J. Chem. Eng. 54 (2016) 101–107, https://doi.org/10.9713/KCER.2016.54.1.101.

[29] L. Madeira, A. Almeida, M. Ribau Teixeira, A. Prazeres, H. Chaves, F. Carvalho, Immediate one-step lime precipitation and atmospheric carbonation as pre-treatment for low biodegradable and high nitrogen wastewaters: a case study of explosives industry, J. Environ. Chem. Eng. 8 (2020) 103808, https://doi.org/10.1016/j.jece.2020.103808.

[30] D.W. Keith, G. Holmes, D. St. Angelo, K. Heidel, A process for capturing CO_2 from the atmosphere, Joule 2 (2018) 1573–1594, https://doi.org/10.1016/J.JOULE.2018.05.006.

[31] S. Viswanaathan, P.K. Perumal, S. Sundaram, Integrated approach for carbon sequestration and wastewater treatment using algal-bacterial consortia: opportunities and challenges, Sustainability 14 (2022) 1075, https://doi.org/10.3390/SU14031075.

[32] D.B. Henthorn, N.A. Peppas, Molecular simulations of recognitive behavior of molecularly imprinted intelligent polymeric networks, Ind. Eng. Chem. Res. 46 (2007) 6084–6091, https://doi.org/10.1021/IE061369L.

[33] Z. Jia, Q. Chang, J. Qin, A. Mamat, Preparation of calcium carbonate nanoparticles with a continuous gas-liquid membrane contactor: particles morphology and membrane fouling, Chin. J. Chem. Eng. 21 (2013) 121–126, https://doi.org/10.1016/S1004-9541(13)60449-8.

[34] L. Ding, B. Wu, P. Luo, Preparation of $CaCO_3$ nanoparticles in a surface-aerated tank stirred by a long-short blades agitator, Powder Technol. 333 (2018) 339–346, https://doi.org/10.1016/J.POWTEC.2018.04.057.

[35] J. García Carmona, J. Gómez Morales, R. Rodríguez Clemente, Rhombohedral–scalenohedral calcite transition produced by adjusting the solution electrical conductivity in the system $Ca(OH)_2$–CO_2–H_2O, J. Colloid Interface Sci. 261 (2003) 434–440, https://doi.org/10.1016/S0021-9797(03)00149-8.

[36] Z. Wang, X. Liu, K. Li, Zhongcheng Wang, Xiaoyu Liu, Ke Li, Study of absorbing CO_2 from emissions using a spray tower, Atmos 13 (2022) 1315, https://doi.org/10.3390/ATMOS13081315.

[37] S. Luz, J. Rivas, A. Afonso, F. Carvalho, Immediate one-step lime precipitation process for the valorization of winery wastewater to agricultural purposes, Environ. Sci. Pollut. Res. (2021) 1–10, https://doi.org/10.1007/s11356-020-11933-3.

[38] A.R. Prazeres, J. Lelis, J. Alves-Ferreira, F. Carvalho, Treatment of vinasse from sugarcane ethanol industry: H_2SO_4, NaOH and $Ca(OH)_2$ precipitations, $FeCl_3$ coagulation-flocculation and atmospheric CO_2 carbonation, J. Environ. Chem. Eng. 7 (2019) 103203, https://doi.org/10.1016/j.jece.2019.103203.

[39] M. Ramalho, T. Jovanović, A. Afonso, A. Baía, A. Lopes, A. Fernandes, A. Almeida, F. Carvalho, Landfill leachate treatment by immediate one-step lime precipitation, carbonation, and phytoremediation fine-tuning, Environ. Sci. Pollut. Res. 1 (2022) 1–10, https://doi.org/10.1007/s11356-022-18729-7.

[40] L. Madeira, F. Carvalho, A. Almeida, M. Ribau Teixeira, Integrated process of immediate one-step lime precipitation, atmospheric carbonation, constructed wetlands, or adsorption for industrial wastewater treatment: a review, Water 15 (22) (2023) 3929, https://doi.org/10.3390/W15223929.

[41] K. Shibata, K. Terasaka, S. Fujioka, K. Kato, Oxygen transfer from a free surface and dispersed bubbles in an aeration tank, J. Chem. Eng. Jpn. 49 (2016) 391–398, https://doi.org/10.1252/JCEJ.15WE180.

[42] T. Correia, M. Regato, A. Almeida, T. Santos, L. Amaral, M. de F.N. Carvalho, Manual treatment of urban wastewater by chemical precipitation for production of hydroponic nutrient solutions, J. Ecol. Eng. 21 (2020) 143–152, https://doi.org/10.12911/22998993/118286.

[43] I. Radovenchyk, I. Trus, V. Halysh, T. Krysenko, E. Chuprinov, A. Ivanchenko, Evaluation of optimal conditions for the application of capillary materials for the purpose of water deironing, Ecol. Eng. Environ. Technol. 22 (2021) 1–7, https://doi.org/10.12912/27197050/133256.

[44] I. Trus, I. Radovenchyk, V. Halysh, E. Chuprinov, D. Benatov, H. Olena, L. Sirenko, Innovative method for water deiron ions using capillary material, J. Ecol. Eng. 23 (2022) 174–182, https://doi.org/10.12911/22998993/145467.

[45] M. Ayoub, Removal of iron and manganese by the fabric capillary action, Int. J. Eng. Sci. 7 (2018) 28–31, https://doi.org/10.9790/1813-0710022831.

[46] R. Deng, X.Z. Xia, J.C. Han, Q.Y. Wu, H.C. Yang, Siphon-driven interfacial photocatalytic reactors enhanced by capillary flow for continuous wastewater treatment, Sep. Purif. Technol. 300 (2022) 121835, https://doi.org/10.1016/J.SEPPUR.2022.121835.

[47] S. Ahmadvand, Behrooz Abbasi, B. Azarfar, M. Elhashimi, X. Zhang, Bahman Abbasi, Looking beyond energy efficiency: an applied review of water desalination technologies and an introduction to capillary-driven desalination, Water 11 (4) (2019) 696, https://doi.org/10.3390/W11040696.

[48] S.J.M. Breig, K.J.K. Luti, Response surface methodology: a review on its applications and challenges in microbial cultures, Mater. Today Proc. 42 (2021) 2277–2284, https://doi.org/10.1016/J.MATPR.2020.12.316.

[49] R. Baird, A.D. Eaton, E.W. Rice, L. Bridgewater, American Public Health Association, American Water Works Association, Water Environment Federation, in: Standard Methods for the Examination of Water and Wastewater, 23rd ed., American Public Health Association, American Water Works Association, Water Environment Federation, 2017.

[50] A.R. Prazeres, J. Rivas, Ú. Paulo, F. Ruas, F. Carvalho, Sustainable treatment of different high-strength cheese whey wastewaters: an innovative approach for

atmospheric CO_2 mitigation and fertilizer production, Environ. Sci. Pollut. Res. 23 (2016) 13062–13075, https://doi.org/10.1007/s11356-016-6429-3.
[51] D. Legendre, R. Zevenhoven, Detailed experimental study on the dissolution of CO_2 and air bubbles rising in water, Chem. Eng. Sci. 158 (2017) 552–560, https://doi.org/10.1016/J.CES.2016.11.004.
[52] M. Yang, T.J. Smyth, V. Kitidis, I.J. Brown, C. Wohl, M.J. Yelland, T.G. Bell, Natural variability in air-sea gas transfer efficiency of CO_2, Sci. Rep. 11 (2021) 13584, https://doi.org/10.1038/s41598-021-92947-w.
[53] J.B. Beigbeder, M. Sanglier, J.M. De Medeiros Dantas, J.M. Lavoie, CO_2 capture and inorganic carbon assimilation of gaseous fermentation effluents using Parachlorella kessleri microalgae, J. CO_2 Util. 50 (2021) 101581, https://doi.org/10.1016/J.JCOU.2021.101581.
[54] J. Liu, B. Li, J. Cao, C. Song, X. Guo, J. Liu, Effects of indium promoter on iron-based catalysts for CO_2 hydrogenation to hydrocarbons, J. CO_2 Util. 65 (2022) 102243, https://doi.org/10.1016/J.JCOU.2022.102243.
[55] Z. Khoobkar, H. Delavari Amrei, A. Heydarinasab, M.A.M. Mirzaie, Biofixation of CO_2 and biomass production from natural gas model using microalgae: an attractive concept for natural gas sweetening, J. CO_2 Util. 64 (2022) 102153, https://doi.org/10.1016/J.JCOU.2022.102153.
[56] M.J. Mitchell, O.E. Jensen, K.A. Cliffe, M.M. Maroto-Valer, A model of carbon dioxide dissolution and mineral carbonation kinetics, Proc. R. Soc. A Math. Phys. Eng. Sci. 466 (2010) 1265–1290, https://doi.org/10.1098/RSPA.2009.0349.
[57] A. Mohammed-Nour, M. Al-Sewailem, A.H. El-Naggar, The influence of alkalization and temperature on ammonia recovery from cow manure and the chemical properties of the effluents, Sustainability 11 (2019) 2441, https://doi.org/10.3390/SU11082441.